Published in final edited form as:
Opt Lett. 2012 May 15; 37(10): 1601–1603.

Targeted alteration of real and imaginary refractive index of biological cells by histological staining

Lusik Cherkezyan[1], **Hariharan Subramanian**[1], **Valentina Stoyneva**[1], **Jeremy D. Rogers**[1], **Seungmoo Yang**[1], **Dhwanil Damania**[1], **Allen Taflove**[2], and **Vadim Backman**[1,*]

[1]Biomedical Engineering Department, Northwestern University, Evanston, Illinois 60208, USA

[2]Electrical Engineering and Computer Science Department, Northwestern University, Evanston, Illinois 60208, USA

Abstract

Various staining techniques are commonly used in biomedical research to investigate cellular morphology. By inducing absorption of light, staining dyes change the intracellular refractive index due to the Kramers-Kronig relationship. We present a method for creating 2-D maps of real and imaginary refractive indices of stained biological cells using their thickness and absorptance. We validate our technique on dyed polystyrene microspheres and quantify the alteration in refractive index of stained biological cells. We reveal that specific staining of individual organelles can increase their scattering cross-section by orders of magnitudes implying a major impact in the field of biophotonics.

Staining provides a tool for visualization of macromolecules, biological cells, and tissues in applications that extend from basic biology to clinical diagnostics [1, 2]. Within the field of optics, the change in light scattering properties of stained organelles caused by the absorption of specific dyes is used to determine their refractive indices [3]. However, while most of the attention has been focused on the absorption (i.e. the imaginary part of refractive index) introduced by staining dyes, the subsequent alteration in the real part of refractive index according to the Kramers-Kronig relation has often been overlooked [4, 5]. A recently proposed linear relationship between the real and imaginary parts of refractive index does not treat the effects of spectral dispersion in either quantity [6]. In this Letter, we demonstrate a method to quantify the wavelength dependent change in both real and imaginary parts of the refractive index of epithelial cells caused by histological stains such as hematoxylin and eosin-containing cytostain.

We construct 2-D maps for real and imaginary refractive indices (n' and n'') of stained cells as a function of wavelength λ as follows: first, we calculate the n'' after measuring the transmission intensity I and the sample thickness L using:

$$I(x,y,\lambda)=I_0(x,y,\lambda_0)\exp\{-(4\pi/\lambda)\int_0^{L(x,y)} n''(x,y,z,\lambda)dz\} \quad (1)$$

where $I_0(x,y,\lambda_0)$ is the transmission intensity at a wavelength λ_0 where absorption is absent (to isolate n'' from other causes of attenuation). For dyes used in this study λ_0= 700nm. Then, we extract the $n'(\lambda)$:

*Corresponding author: v-backman@northwestern.edu.

$$\begin{aligned} n'' &= \chi''_{dye}/2n' \\ n' &= n_0\sqrt{1+\left(\chi'_{dye}+n''^2\right)/n_0^2} \end{aligned} \tag{2}$$

where $\chi'_{dye}+j\chi''_{dye}$ is the electric susceptibility of dye molecules embedded in a nonabsorbing material with a refractive index n_0; χ'_{dye} is determined from χ''_{dye} using Kramers-Kronig relations [4, 5, 7]:

$$\begin{aligned} \chi'_{dye}(k) &= (2/\pi)P\int_0^\infty k'\,\chi''_{dye}(k')/\left(k'^2-k^2\right)dk' \\ \chi''_{dye}(k) &= -(2k/\pi)P\int_0^\infty \chi'_{dye}(k')/\left(k'^2-k^2\right)dk' \end{aligned} \tag{3}$$

where P denotes Cauchy principal value and k is the wavenumber $k=2\pi/\lambda$. Our instrumentation includes an atomic force microscope (AFM, Bruker Bioscope II) with 39 nm resolution to measure the thickness $L(x,y)$ and a custom built spectroscopic microscope (SM) to image the sample, as well as measure the wavelength dependent transmission through it $I(x,y,\lambda)$. The sample of interest is mounted between 2 glass slides using Permaslip (Alban Scientific) to remove specular reflections at the specimen-air interface. The bottom glass slide is coated with a 100nm layer of Aluminum (Deposition Research Lab) in order to redirect the transmitted light back through the sample onto the detector (Fig. 1). Thus, the recorded signal (normalized by the reflectance of a mirror) represents transmission after a double pass through the sample which effectively increases its thickness and therefore the signal-to-noise ratio of absorption measurements.

In order to establish this SM-based technique as a method for recovering refractive index change after staining, we first tested a controlled phantom. The phantom consisted of dry red-dyed polystyrene microspheres suspended in a droplet of permaslip between 2 glass slides (Polybead, diameter a = .2μm) as illustrated in Fig. 1a. To account for the difference between the dye distribution within this phantom and within a stained cell, we transformed Eq. 1 into an analogous expression for a suspension of spheres with absorption efficiency $Q_{abs}(\lambda)$ and total number per voxel $N(x,y)$: $I(x,y,\lambda) = I_0 \exp(-N(x,y)\pi\,(\alpha/2)^2\,Q_{abs}(\lambda))$. Thus, after the transmission spectrum was acquired by SM, the $Q_{abs}(\lambda)$ was obtained. This determined both parts of the dyed sphere complex refractive index ($n(\lambda)$): the $n''(\lambda)$ was reconstructed from: ([8])

$$\mathrm{Im}\left\{\frac{n^2(\lambda)-n_{med}^2(\lambda)}{n^2(\lambda)+2n_{med}^2(\lambda)}\right\} = -\frac{\lambda}{8\pi a}Q_{abs}(\lambda) \tag{4}$$

where Im denotes imaginary part of a complex variable, and “med” refers to the surrounding medium; the $n'(\lambda)$ was obtained from Eq. 2 with n_0 corresponding to unstained (white) polystyrene. Note that unlike the $n(x,y,\lambda)$ of a biological cell, the n of a polystyrene sphere is independent of location (x,y).

To verify the reliability of extracted $n'(\lambda)$ and $n''(\lambda)$ of dyed spheres we quantified them independently with the integrating sphere (IS) technique. As the IS required a large homogeneous sample, the spheres were suspended in water instead of the rapidly solidifying permaslip. After the transmittance and reflectance were measured with IS, the absorption and reduced scattering coefficients were recovered by inverse Adding-Doubling (IAD) [9–11] algorithm and normalized by known sphere concentration. Eq.4 was then used to calculate n''. The $n''(\lambda)$ and the reduced scattering cross-section σ'_{sca} of dyed microspheres obtained by both SM and IS-IAD are shown in Fig. 2. Spectral profiles of n'' show good

agreement within one standard error of each other with a 7nm peak shift noticeable from 555 to 575 nm (Fig. 2a). This can be attributed to the chemical interactions of the dye with different solvents (water and permaslip). Since n' alone cannot be calculated using IS-IAD, we instead compared the σ'_{sca} as it is defined by both n' and n''. The corresponding σ'_{sca} for the SM was recovered using Mie theory ([12]). A perfect match between the σ'_{sca} obtained by both IS-IAD and SM is seen in Fig. 2b. These results confirmed the reliability of our technique in measuring complex refractive index of dyed materials.

Next, we quantified the complex refractive index of stained squamous epithelial cells extracted from buccal mucosa. The cells were smeared onto the metallic surface of coated slides using a cytobrush (CooperSurgical), fixed with 95% ethanol and stained with conventional nuclear and cytoplasmic dyes: hematoxylin (H) (absorption peak at 628nm) and Cytostain (absorption peak of eosin (E) at 536nm) (Richard-Allan, Thermo Scientific). Cell thickness was obtained using AFM, after which a glass slide was mounted on top of the sample as described above. To calculate n' and n'' of a stained cell using Eq. 2, the refractive index of an unstained cell (n_0) is required. Although the reported refractive index of dehydrated cells is between 1.50 and 1.55 [13, 14], the exact values are poorly investigated. In this study we evaluated n_0 using Gladstone-Dale relation $n=n_w+\alpha\rho$ where n_w is the refractive index of water, α is the specific refractive increment (0.18ml/g), and ρ is the cell dry density which was approximated as that of stratum mucosum (1.15 g/ml) [15]. This resulted in the average $n_0(\lambda)$ of 1.54 (Fig. 3b).

As a demonstration, we subsequently evaluated $n'(\lambda)$ and $n''(\lambda)$ of three squamous epithelial cells. The absorption strength greatly varied between them and the average peak values of the measured $n''(\lambda)$ were 0.05, 0.06, and 0.08. In response, according to Kramers-Kronig relations (Eq. 3), the $n'(\lambda)$ decreased at λ shorter than the absorption peak and increased at λ longer than the absorption peak by 0.06, 0.08, and 0.11 respectively. Thus, we revealed that the change in the intracellular refractive index induced by staining is significantly greater than the reported endogenous spatial variations of it (0.02, [16]).

The summary of results from a typical cell is illustrated in Fig. 3. Note that the refractive index maps represent vertically averaged values and thus inherently underestimate its spatial variations. For instance, consider the voxel circled in red that includes nucleus surrounded by cytoplasm layers from above and below. The spectrum of $n''(\lambda)$ corresponding to it has peaks at the absorption wavelengths of both H and E. Its magnitude at 536nm suggests a lower effect of E in that region compared to the purely cytoplasmic voxels (blue and orange). However, this is a sheer consequence of averaging throughout the volume where E is not distributed homogeneously. Similarly, since the affinity of dye molecules is determined by their chemical properties, it is not uniformly spread within a biological cell. As a result, the refractive index change at the site of their localization is larger than when averaged throughout the cell thickness.

Of particular importance is that by changing the spatial distribution of refractive index, staining significantly affects the extinction properties of intracellular compartments. As an illustration, using the Mie theory [12] we calculated the absorption and scattering efficiencies of spheres with refractive indices before and after staining corresponding to the black and orange spectra in Fig. 3b. As seen in Fig. 3d, while the staining-induced absorption efficiency increases with particle size, in contrast the amplification of the scattering efficiency decreases. Moreover, for intracellular particles such that $ka(n_{particle}/n_{med}-1)<<1$, introduction of n'' can amplify their scattering cross-sections by orders of magnitudes [17]. Interestingly, with the increase of sphere diameter, the spectral profile of the scattering amplification gradually changes from resembling the spectral shape of $n''(\lambda)$ into resembling that of the $n'(\lambda)$ as also was predicted in Ref. 8.

In conclusion, while the absorption of staining dyes is used in routine microscopy, its imaging resolution is diffraction limited. Meanwhile, the refractive index change demonstrated here suggests an alternative use of dyes as contrast agents in the field of light scattering to investigate subdiffractional structures such as specific organelles, chromatin fibers, proteins, etc. In clinic, this effect can advance cancer diagnosis when utilized by scattering-based techniques such as optical coherence microscopy (OCM), light scattering spectroscopy (LSS), confocal light absorption and scattering spectroscopy (CLASS), and partial wave spectroscopic (PWS) microscopy [18, 19].

Acknowledgments

This work was supported by National Institutes of Health (NIH) grants R01CA128641, R01EB003682, and R01CA155284, and National Science Foundation (NSF) grant CBET-0937987.

References

1. De Robertis, EDP.; Saez, FA.; De Robertis, EMF. Cell biology. 6th ed.. Philadelphia: Saunders; 1975. p. xvp. 615
2. Cibas, ES.; Ducatman, BS. Cytology : diagnostic principles and clinical correlates. Philadelphia: W.B. Saunders; 1996. p. xivp. 371
3. Wilson JD, Cottrell WJ, Foster TH. Index-of-refraction-dependent subcellular light scattering observed with organelle-specific dyes. Journal of Biomedical Optics. 2007; 12:014010. [PubMed: 17343485]
4. Kramers HA. La diffusion de la lumi'ere par les atomes. Atti del Congresso Internazionale dei Fisici. 1927; 2:545–557.
5. Kronig, RdL. On the theory of dispersion of X-rays. Journal of Optical Society Of America. 1626; 12:547–556.
6. Uttam S, Bista RK, Hartman DJ, Brand RE, Liu Y. Correction of stain variations in nuclear refractive index of clinical histology specimens. Journal of Biomedical Optics. 2011; 16:116013. [PubMed: 22112118]
7. Lucarini, V. Kramers-Kronig relations in optical materials research, Springer series in optical sciences. Berlin ; New York: Springer; 2005. p. ixp. 160
8. Hulst, HCvd. Light scattering by small particles, Structure of matter series. New York: Wiley; 1957. p. 470
9. Prahl SA. Inverse Adding-Doubling Software. http://omlcogiedu/software/iad/index.html.
10. Pickering JW, Prahl SA, Vanwieringen N, Beek JF, Sterenborg HJCM, Vangemert MJC. Double-Integrating-Sphere System for Measuring the Optical-Properties of Tissue. Appl Optics. 1993; 32:399–410.
11. Prahl SA, Vangemert MJC, Welch AJ. Determining the Optical-Properties of Turbid Media by Using the Adding-Doubling Method. Appl Optics. 1993; 32:559–568.
12. Maetzler, C. MATLAB Functions for Mie Scattering and Absorption. Bern, Switzerland: Institut fur angewandte Physik, Universitaet Bern; 2002.
13. Cook, DJ. Cellular Pathology. 2 ed.. Bloxham: Scion Publishing Ltd; 2006. Staining Theory; p. 350
14. Crossmon GC. Mounting media for phase microscope specimens. Stain Technol. 1949; 24:241–247. [PubMed: 18149090]
15. Davies HG, Wilkins MHF, Chayen J, Lacour LF. The Use of the Interference Microscope to Determine Dry Mass in Living Cells and as a Quantitative Cytochemical Method. Q J Microsc Sci. 1954; 95 271-&.
16. Schmitt JM, Kumar G. Optical scattering properties of soft tissue: a discrete particle model. Appl Optics. 1998; 37:2788–2797.
17. Kattawar GW, Plass GN. Electromagnetic scattering from absorbing spheres. Appl Opt. 1967; 6:1377–1382. [PubMed: 20062208]

18. Boustany NN, Boppart SA, Backman V. Microscopic imaging and spectroscopy with scattered light. Annu Rev Biomed Eng. 2010; 12:285–314. [PubMed: 20617940]

19. Subramanian H, Pradhan P, Liu Y, Capoglu IR, Rogers JD, Roy HK, Brand RE, Backman V. Partial-wave microscopic spectroscopy detects subwavelength refractive index fluctuations: an application to cancer diagnosis. Optics letters. 2009; 34:518–520. [PubMed: 19373360]

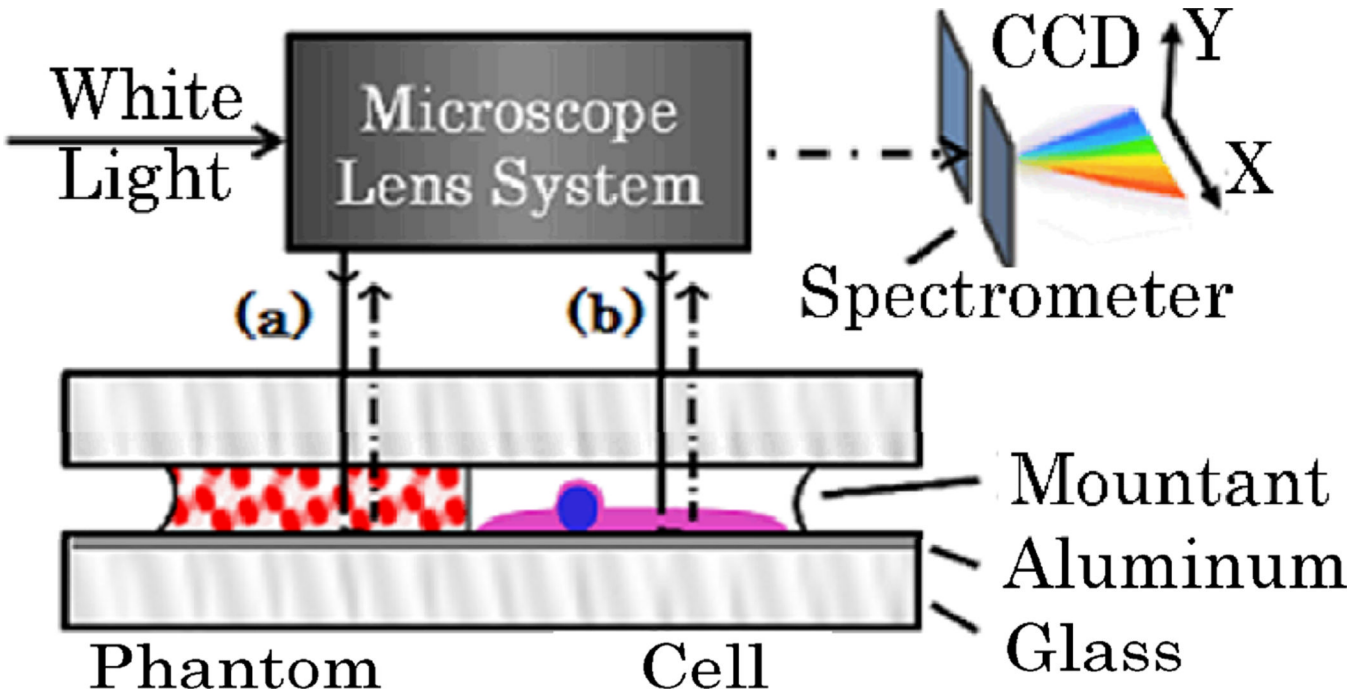

Fig. 1.
Schematic of the SM and sample design: reflected-light Kohler illumination brightfield microscope (60× objective lens; N.A. 0.4) projects sample image through a grating spectrometer on a CCD camera. A stage under the spectrometer spatially scans the sample image. [a] dyed microsphere phantom and [b] stained biological cell.

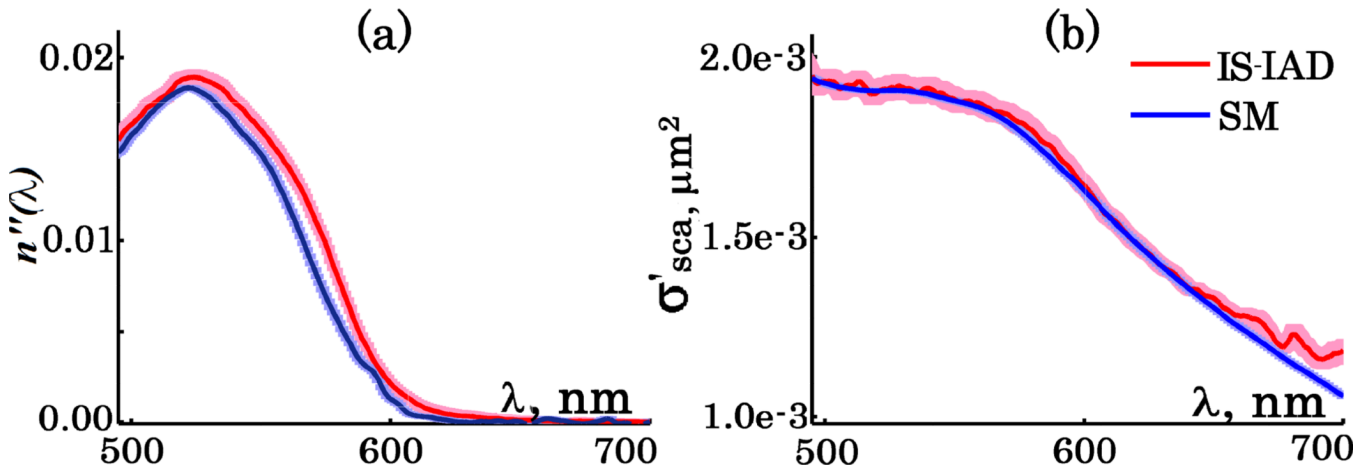

Fig. 2.

[a] n'' of dyed polystyrene microspheres and [b] their reduced scattering cross-section. IS-IAD data in red and based on post-processing of the SM measurements in blue. Standard errors in corresponding shaded colors.

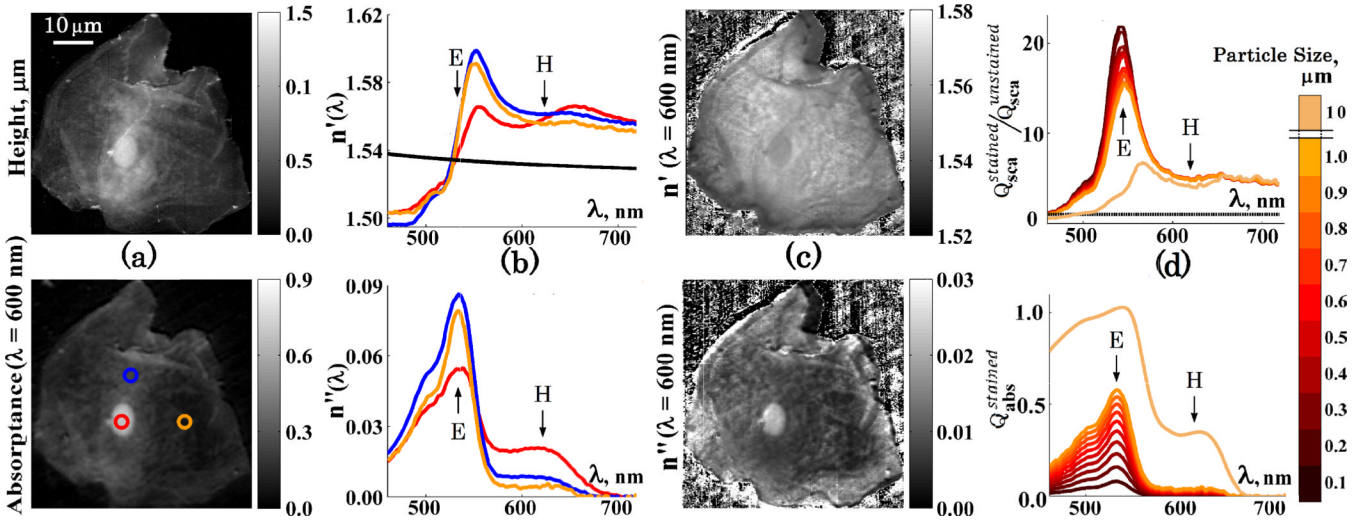

Fig. 3.

[a] shows the measured cell height and absorptance at 600nm; [b] illustrates the *n'* and *n"* for 3 areas (black corresponds to unstained), letters H and E point to the absorption peaks of hematoxylin and eosin correspondingly; [c] illustrates the spatial dis tribution of *n'* and *n"* at 600nm within the cell; [d] size-dependent absorption efficiency (Q_{abs}) and amplification of scattering efficiency (Q_{sca}) (refractive index of surrounding medium assumed to be 1.52).